

Article

Experimental and Numerical Investigations of RC Frame Stability Failure under a Corner Column Removal Scenario

Sergey Savin ^{1,*} , Vitaly Kolchunov ¹, Natalia Fedorova ² and Ngoc Tuyen Vu ²

¹ Department of Reinforced Concrete and Masonry Structures, Institute of Civil Engineering, National Research Moscow State University of Civil Engineering, 129337 Moscow, Russia

² Department of Architectural and Structural Design, Mytishchi Branch of National Research Moscow State University of Civil Engineering, National Research Moscow State University of Civil Engineering, 129337 Moscow, Russia

* Correspondence: savinsyu@mgsu.ru; Tel.: +7-920-812-5909

Abstract: In recent decades, interest in the resistance of buildings and structures to progressive collapse has been increasingly sparked in research communities. Although several experimental, numerical, and analytical research projects on the robustness of building frames under a column removal scenario have been implemented, some aspects of this problem remain understudied. These aspects encompass failure mechanisms of reinforced concrete frames with slender columns, as well as criteria used to evaluate such failures. This paper focuses on experimental and numerical investigations of the structural behavior and failure of a scale reinforced concrete frame with slender columns under a sudden corner column removal scenario. In addition, we analyze the stability failure mechanism of a reinforced concrete frame with slender columns and the tangent stiffness criterion, which allow for evaluation of the ultimate state of a structure subjected to an accidental impact. A scale physical model of a reinforced concrete frame of a multistory building was designed and tested using the theory of functional similarity. For numerical study purposes, a finite element model was made that exactly the same as the test frame. We validated the findings by comparing simulation results and experimental data. The studies on the behavior of a reinforced concrete frame subjected to quasistatic loading with unequal concentrated loads identified the load transfer between columns through beams. Although these effects were minor in the frame under consideration, they can become more significant in cases of long-term loading. Numerical simulation and physical modeling of an accidental impact allowed for identification of the mechanism of load capacity exhaustion triggered by stability failure. Such failure was fragile. The moment of stability failure of the column of the experimental frame corresponded to the extremum on the force–displacement curve, indicating that zero tangent stiffness was reached. Hence, a criterion of tangent stiffness can be proposed for evaluation of the ultimate state of a structure subjected to an accidental impact.

Keywords: reinforced concrete frame; slender column; corner column removal; progressive collapse; robustness; stability failure



Citation: Savin, S.; Kolchunov, V.; Fedorova, N.; Tuyen Vu, N. Experimental and Numerical Investigations of RC Frame Stability Failure under a Corner Column Removal Scenario. *Buildings* **2023**, *13*, 908. <https://doi.org/10.3390/buildings13040908>

Academic Editor: Elena Ferretti

Received: 10 March 2023

Revised: 23 March 2023

Accepted: 24 March 2023

Published: 29 March 2023



Copyright: © 2023 by the authors. Licensee MDPI, Basel, Switzerland. This article is an open access article distributed under the terms and conditions of the Creative Commons Attribution (CC BY) license (<https://creativecommons.org/licenses/by/4.0/>).

1. Introduction

1.1. Literature Review

In recent decades, the problem of resistance, robustness, and structural integrity of buildings under accidental impacts caused by the removal of a load-bearing member of a structural system has attracted considerable interest in the scientific literature on structural engineering [1–3]. Despite the low probability of such accidents, the risk associated with their consequences for the mechanical safety of buildings and structures, as well as human life and health, may be substantial [4–6]. Therefore, they should be analyzed at during the design and reconstruction phases of facilities belonging to high-risk categories, especially those with high occupancy rates. Real-life accidents, such as the partial collapse of the

Ronan Point Building as a result of a gas explosion [7], the collapse of a condominium in Surfside [8], destruction caused by the terrorist attack on the Alfred Murray federal building [9], or the case of the Transvaal Park collapse [10], show that causes and mechanisms of collapse vary extensively. Kiakojoury et al. [11] focused on design and construction errors; evolutionary accumulation of environmental and mechanical damage; natural hazards such as tornadoes, hurricanes, earthquakes, and tsunamis; acts of terrorism, etc. In this regard, codes and standards issued by US General Services Administration (GSA) and the Department of Defense (DoD) [12,13] (ASCE/SEI-7-16 [14], EN-1991-1-7 [15], SP 385.132580 and GOST 27751-2014 [16,17], etc.) adopt a situational approach to ensure facility resistance to progressive collapse in the case of the failure of a structural member due to an impact of unknown nature.

Analysis of experimental, numerical, and analytical studies on resistance of structural systems and their test models under a load-bearing element removal scenario indicates that the load redistribution, which involves alternative loading paths, may occur quite quickly, causing dynamic effects. When considering the reasons and mechanism of collapse of the World Trade Center, Bazant et al. [18] argued that the initial mechanical damage caused by the collision of the aircraft with the facility, coupled with the fire action, triggered a catenary mechanism of resistance of the floor slabs. As a result, deflected floor slabs pulled the columns, which led to their buckling. To assess the possibility of destruction propagation, the authors proposed a one-dimensional dynamic model and an energy criterion. Having studied reports on the Ronan Point collapse, Pearson et al. [7] assumed that a relatively small gas explosion on the 18th floor of the building led to the failure of the precast element of the load-bearing wall, which served as a single support for the structures of the upper floor. Dynamic effects caused by the fall of the four upper floors destroyed the load-bearing structures of the 17th floor and triggered the fall of subsequent floors of the building all the way through its base. Belostotsky and Pavlov [10] presented the results of numerical simulation of the structural behavior of elements of the load-bearing system of Transvaal Park. They concluded that one of the possible reasons for the collapse was the local buckling of the column due to the push action of the brace element. The second possible reason was the failure of the roof-to-column joint. The results of their study confirmed the need to take into account the effects of physical, geometric, and constructive nonlinearities of nodes, elements, and systems in the process of their design. Tagel Din et al. [9] compared the complete picture of the Alfred Murray federal building collapse with a simulation based on the elemental method. Simulation results allowed them to reconstruct the following timelines of destruction propagation. Column G20 collapsed 0.3–0.4 s after the blast due to the action of the blast wave. Then, destruction propagation stopped for 1.5 s, after which partial collapse of the building continued for 4.5 s. Kong et al. [8] use video processing of the collapse of the Surfside condominium to identify five characteristic stages of destruction. The duration of the first stage of destruction was about 0.04 s. After 0.4 s, the damaged area increased and spread to new areas of the load-bearing system of the building as a result of the redistribution of loads.

The above-mentioned building codes allow for the application of various methods of analysis of alternative loading paths, such as dynamic time-history analysis, quasistatic analysis, and the static approach. The dynamic time-history analysis of resistance of multi-story buildings to progressive collapse was considered in the works of Kwasniewski [19], Yousef and El-Mandouh [20], etc. The complexity of this approach lies in the limited amount of data on the time of force redistribution and dynamic patterns of building failures, especially when it comes to accidents that occurred several decades ago. The DoD [13] and GSA [12] suggest assuming that the force redistribution time is not less than 1/10 of the period of vibrations for the mode triggered by the strain state following the impact under consideration. SP 385.132580 [16] and EN [15] provide no guidance in this regard. The quasistatic method was considered by Almazov et al. [21], Kabantsev and Mitrovic [22], Mohamed and Keshawarz [23], etc. This method applies the static equivalent of dynamic effects. It requires experimental substantiation of the impact effects on the building frame

in the case of removal of a load-bearing element. The static method, as considered by Kodysh et al. [24] and SP 385.132580 [17], assumes a lack of significant dynamic effects on structures because of the inelastic behavior and damping of multistory reinforced concrete building frames. In addition, it is noteworthy that, as a rule, most of studies focus on the problem of a building's resistance to progressive collapse [1,2,25] and evaluate the robustness of beams, slabs, and roofs above the collapsed structural element. Some researchers have studied a reduction in a structural member's loading capacity due to a reduction in the strength and stiffness properties of the material exposed to environmental impacts [18,26]. Kiakojouri et al. [11] argued that the zipper, pancake, and domino types of progressive collapse may occur even if the arch [27], membrane [28], or Vierendeel truss resistance mechanism [29] is triggered for beam and slab structures above a collapsed structural element or ties. The occurrence of these failure mechanisms depends on the slenderness of load-bearing elements, the ratio of their stiffness, and boundary conditions. However, it seems that there are no quantitative criteria to clarify which of them may occur in the case of the specified parameters of the building frame and actions on it.

Sasani and Sagiroglu [30] tested a six-story San Diego hotel building prepared for demolition to evaluate the resistance of its frame to progressive collapse. Analysis of readings of the strain gauge installed on the opposite sides of the first-floor column, which was next to the removed column, showed that the dynamic effects were about 1.9 and 1.4 times the values measured following the decay of vibrations, indicating a quantitative and qualitative change in the stress–strain state of the column as a result of the structural transformation of the building frame after corner column failure. The absence of substantial damage in the tested frame was due to the lack of live loads on the floor slabs and roof. It should also be noted that the slenderness ratio ($\lambda_{hi} = l_0/h$) of the column was in the range of 8 to 10 in this test. Kolcunov et al. [31], Zheng et al. [32], Shan and Li [33], Yang et al. [34], Fedorova and Vu [35], and Adam et al. [36] tested scale and full-size reinforced concrete frames for which the slenderness ratio of the columns did not exceed $\lambda_{hi} = 6$. Tamrazyan and Avetisyan [37] and Popov [38] studied the resistance of eccentrically compressed columns with a slenderness ratio of about $\lambda_{hi} = 6$ under environmental action and dynamic loading. As a rule, the bearing capacity of reinforced concrete columns with such a slenderness ratio mainly depends on the cross-sectional strength, and second-order effects are small. Numerical studies of the dynamic response of reinforced concrete columns, depending on their slenderness ratio [39], show that an increase in the slenderness ratio (λ_{hi}) greater than 10 leads to a more intensive deflection increase and, accordingly, an increase in second-order moments. This circumstance requires consideration of integral criteria, assessing the special limiting state [17] of compressed and eccentrically compressed columns of building frames, in addition to the existing criteria of cross-sectional strength. Sanzharovsky [40], Golyshev and Kolchunov [41], and others proposed a criterion of tangent stiffness as an integral criterion, evaluating the resistance of eccentrically compressed elements of reinforced concrete frames. Gemmerling [42] considered that criterion for evaluation of the stability failure of inelastic bar structural elements of frame structures. He also proposed applying this criterion to the evaluation of the post critical behavior of a bar with negative tangent stiffness. The tangent stiffness criterion was also applied for the analytical assessment of resistance of reinforced concrete frames to progressive collapse [43] under a support removal scenario. The authors of [44] discussed a possible design of a scale model of a reinforced concrete frame within the framework of an experimental study. A preliminary quasistatic analysis was conducted, in which finite elements of the beam type were used to simulate a frame fixed entirely out of plane. In that numerical study, dynamic effects were evaluated using the approximate energy approach proposed by Geniyev [45]. Therefore, it seems that there has been no experimental substantiation of this criterion and its application to the evaluation of resistance to progressive collapse.

1.2. Purpose, Objective, and Summary of the Study

The analysis of the current state of research on the problem of progressive collapse of buildings provided in Section 1.1 allows us to conclude that there are no data available on failure mechanisms of frames with slender columns under accidental impacts. Thus, the objective of this study is the investigation of the failure mechanism of a reinforced concrete frame with slender columns and tangent stiffness criteria to evaluate the ultimate state of a structure under an accidental impact.

To achieve the presented study objectives, a physical model of a building frame was proposed based on functional similarity. Principles and limitations underlying physical modeling are described in Section 2.1. Furthermore, in Section 2.2 of this article, the design of an experimental frame and the technology of its manufacture, as well as physical and mechanical properties of materials, are described. The test method and equipment used in this study are provided in Section 2.3. Section 3 presents the results of an experimental study and numerical simulation of the structural behavior of a reinforced concrete frame under a corner column removal scenario. Section 3.1 shows the experimental load–displacement graphs for the first stage of the test, when the corner column is in the frame. In this subsection, we also present video processing data for the second stage of the test when the corner column removal occurs. Displacement histories are provided for the frame joints. Post-testing images of the failure mechanism of reinforced concrete frame joints are also provided. Section 3.2 describes numerical simulation assumptions, including the types of finite elements, boundary conditions, material of models, and criteria for evaluating the ultimate state of the frame. The finite element model was evaluated by comparing the results of physical and numerical modeling. The failure mechanism and appropriateness of the tangent stiffness criterion are also analyzed in this subsection.

The scientific novelty of the present study lies (1) in obtaining new data on experimental and numerical research into the failure mechanism of a reinforced concrete frame with slender columns under a sudden corner column removal scenario, as well as (2) in evaluating the applicability of the tangent stiffness criterion to the analysis of the ultimate state of structural elements.

2. Materials and Methods

2.1. Method for Physical Modeling

The disproportionate collapse of a structural system after a sudden removal of a structural member is a rather complex phenomenon. Therefore, extensive resources are often required to verify and evaluate numerical models. In this regard, the functional similarity method was applied. This method is expedient in analyzing physical and numerical models at various levels.

The application of functionally similar physical models is considered a way to verify the adequacy of numerical models of the non-linear behavior of reinforced concrete structural systems under complex loading conditions. Physical models are developed for this purpose on the basis of fully functional similarity between a test model and a real building frame under a sudden column removal scenario.

The confirmation of the adequacy of a numerical model of a structural element requires physical simulation. At the same time, a combination of functional, simple, or extended similarity allows for determination of the stiffness and strength parameters of a structural element or a joint [46–48]. Thus, the principle of mixed similarity is applied to experimental physical models. The overall test model of a reinforced concrete frame is functionally similar to the design scheme of a full-scale building frame subjected to corner column removal. Structural members and joints of the test model are related to the real building frame in accordance with the simple similarity principle. This means similarity of geometry, boundary conditions, scale factors, equality of mechanical properties of the material, quantitative and qualitative similarity of the impact parameters, etc. Bazant and Kwon [49] argued that the scale factor affects the cracking pattern and damage propagation in structural elements. However, failure mechanisms of structural elements and their

models are quite similar. Thus, the use of scale models is acceptable for analysis of failure mechanisms and evaluation of the load capacity criteria.

Comparative analysis of modeling conditions, which is performed using similarity types [46–48], allows for recommendations with respect to the application of a functionally similar physical model for which the following conditions are satisfied:

- Physical phenomena have the same nature in terms of physical and numerical simulation;
- The physical model and the real building frame have a similar design model;
- The number of determining similarity criteria is the same for the model and the full-scale structure, although their numerical values may differ;
- Physical and mechanical properties of materials are the same for the model and the real facility;
- The loading pattern of the physical model may differ slightly from that of the real structure; however, the nature of the stress–strain state of elements of the model and the real facility should be similar.

2.2. Design of the Test RC Frame and Mechanical Properties of Materials

A scale two-story reinforced concrete frame was manufactured for the purpose of this research. The design of this frame is presented in Figure 1.

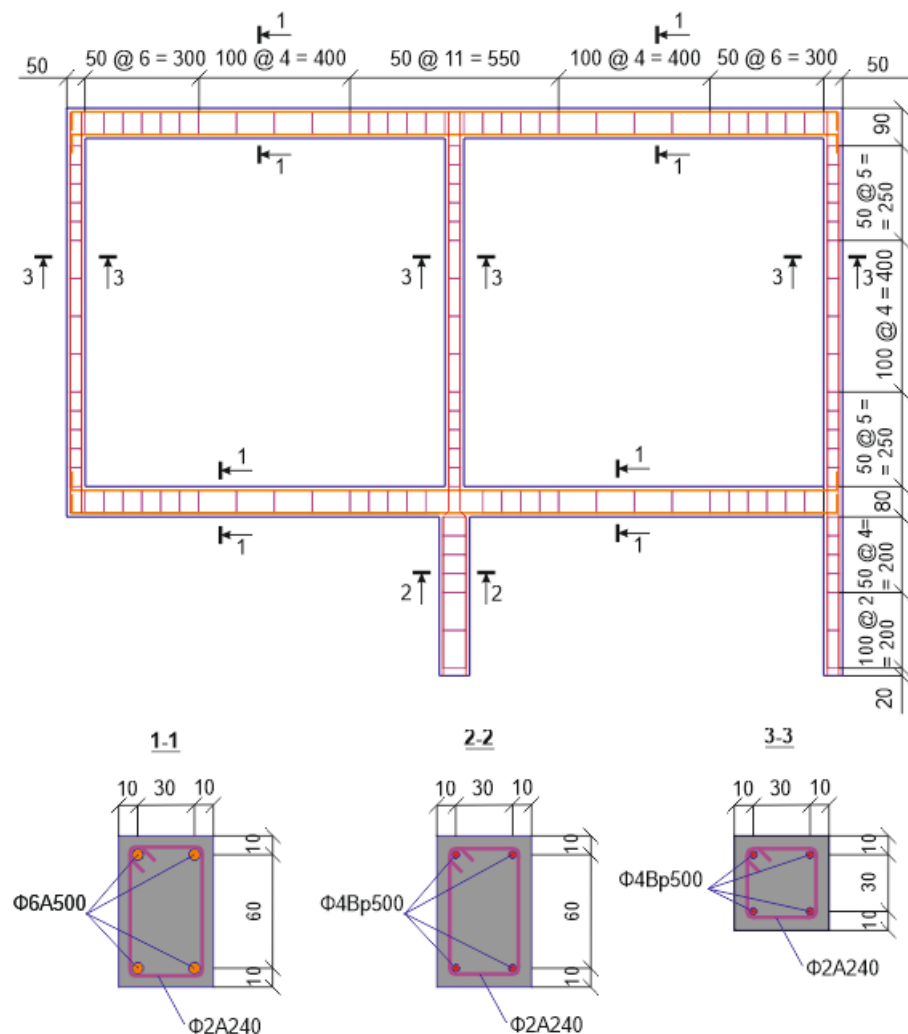


Figure 1. Design of the reinforced concrete test frame: the reinforcement.

The scale of the experimental frame was assumed to be about one to eight with respect to a possible full-scale frame design. The slenderness ratio of columns in the plane of

the frame is $\lambda_{hi} = 22$ ($\lambda_i = 76.1$), which does not exceed the limit value set by regulations ACI-318-19 [50] and SP 63.13330 [51]. Columns with such a high slenderness ratio can be found in buildings with large halls, such as philharmonic halls, theaters, cinemas, etc. Given their functional purpose, such buildings imply simultaneous mass gatherings of people. Therefore, it is important to study the resistance of load-bearing systems of such buildings to progressive collapse. Cross-sectional dimensions of the beams were adopted in this study to ensure the resistance of structures above the lost support according to the Vierendeel truss scheme.

Since the scale ratio of the frame is relatively large, principles of similarity addressed in the works written by Kirpichev [46] and Sedov [47] and applied together with the approximate size effect law proposed by Bazant and Kwon [49] should be considered for the transition to a real-size structure. However, issues of transition to a real-size structure are beyond the scope of this article. This study is limited to experimental and numerical investigations of effects produced on the scale model only.

The concrete mixture was placed in a horizontal formwork and compacted using vibration. Vibration was created by a perforator through a wooden plate installed on the bottom sheet of the formwork. Compaction was continued until air bubbles disappeared from the surface of the concrete mixture. Figure 2a,b show the formwork with reinforcement cages and with the concrete mixture after compaction. Simultaneously with the concreting of the test frame, we produced benchmark specimens: three $100 \times 100 \times 100$ mm cubes for the preliminary determination of compressive strength and three $100 \times 100 \times 400$ mm prisms to plot the stress–strain diagrams under uniaxial compression, as presented in Figure 2c,d.

The specimens were cured in a chamber for 28 days, after which they were tested in hydraulic presses to ensure the strength parameters. The tensile strength was identified indirectly according to the analytical relationship with compressive strength [52]. The composition of the concrete mixture for the test frames was set to ensure a characteristic compressive strength of the concrete cubes of about 25 MPa (Table 1).



Figure 2. Cont.

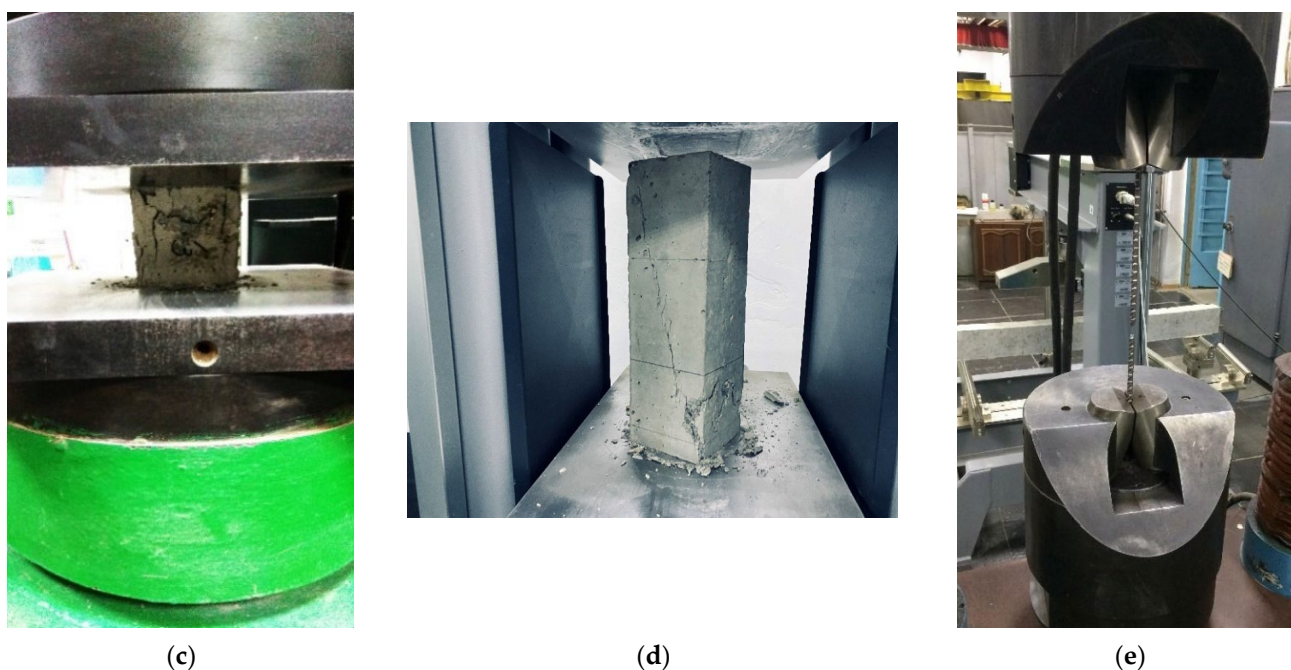


Figure 2. General view of the formwork with the reinforcement (a); general view of the test frame formwork after concreting (b); testing of the specimens: concrete cube (c), concrete prism (d), reinforcement steel bar (e).

Table 1. Composition of concrete mixture.

Portland Cement M400, kg/m ³	Crushed Diorite Stone from the Lozovsky Quarry; Grain Size 5–10 mm, kg/m ³	Washed Sea Sand; Grain Size 2–2.5 mm, kg/m ³	Plasticizer Master Glenium 3045	Water (W/C = 0.4), kg/m ³
450	1155	655	1%	180

The frame was reinforced with spatial cages in a symmetrical arrangement of longitudinal reinforcement bars, as shown in Figure 1. The columns were longitudinally reinforced with cold-formed steel bars (4 Ø 4 Bp500) with an average yield strength of 526.5 MPa identified experimentally using an MP-500 tensile testing machine, as presented in Figure 2e. Hot rolled steel bars (4 Ø 6 A500) with an average yield strength of 606.4 MPa were installed symmetrically into reinforcement girder cages. Stirrups were made of smooth wire with a diameter of 2 mm and an average yield strength of 317.1 MPa. Material properties of the steel reinforcement are presented in Table 2.

Table 2. Mechanical properties of steel reinforcement.

Reinforcement Steel Bars	Diameter, mm	Modulus of Elasticity, GPa	Yield Stress, MPa	Ultimate Stress, MPa
A500	6	200	606,4	680
Bp500	4	200	526,5	584
A240	2	200	317,1	440

For the preliminary evaluation of the compressive strength of concrete prisms, benchmark cubes were tested with a P-125 hydraulic press with a measurement range of 0 to 125,000 kgf (1225.8 kN) using the method described in GOST 10180-2012 [53] for a loading rate of (0.6 ± 0.2) MPa/s.

Concrete prisms were tested with a C8422 hydraulic press, and loading was broken down into steps of 20% of the anticipated axial compressive strength with a loading rate

of (0.6 ± 0.2) MPa/s. After each step, the specimen was subjected to constant loading for 2 min. Tables 3 and 4 present the material properties of the concrete cubes and prisms in accordance with the requirements of GOST 10180 [53] and GOST 18105 [54].

Table 3. Test results for concrete cubes.

Specimen Index	Cross-Sectional Area, cm ²	Density, kg/m ³	Ultimate Load, kN	Scale Factor (α)	Strength (R), MPa	Strength Class for Concrete
C3-1	101.0	2338	364.2	0.95	34.3	B25
C3-2	102.9	2311	369.1		34.1	
C3-3	100.5	2324	354.6		33.5	
Average compressive strength (R_m), MPa					34.0	
Coefficient of variation, %					2.1	
Actual compressive strength class for concrete					27.2	

Table 4. Test results for concrete prisms.

Specimen Index	Compressive Strength of Prisms, MPa	Initial Modulus of Elasticity of Concrete (E_0), MPa	Compressive Strain in the Concrete at Peak Stresses, $\epsilon_{c0} \cdot 10^6$
P3-1	25.5	23,330	2310
P3-2	24.7	25,760	2170
P3-3	25.4	25,770	2090
Average value	25.2	24,950	2190

Figure 3 shows the stress–strain diagrams for concrete prisms and cubes under uniaxial compression.

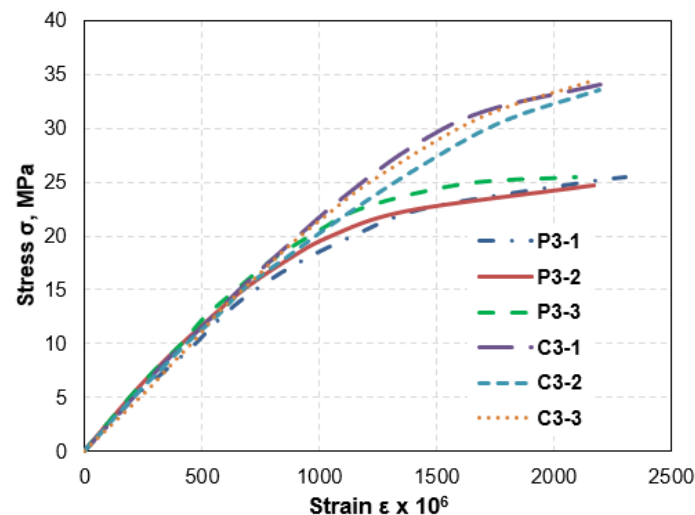


Figure 3. Stress–strain diagrams for concrete prisms (P3-1, P3-2, and P3-3) and cubes (C3-1, C3-2, and C3-3) under uniaxial compression.

2.3. Test Method

The reinforced concrete frame was installed in a test bench as presented in Figure 4a. First-floor columns represented a fixed hinge. A general view of the frame specimen installed on the test bench is shown in Figure 4b. The loading pattern and boundary conditions are presented in Figure 4c. Out-of-plane displacements of the test frame were limited by bilateral linear ties in the upper beam-to-column joints, but they allowed for the free motion of the test structure in the plane. This tie was a $560 \times 50 \times 50$ mm wooden beam,

which limited the displacement of the frame towards the concrete wall. The displacement from the wall was limited by a steel cable with a diameter of 4 mm, which was installed without tension to enable the motion of the frame specimen in the plane. Thus, the stiffness of the tie was at least 1.2 MN.

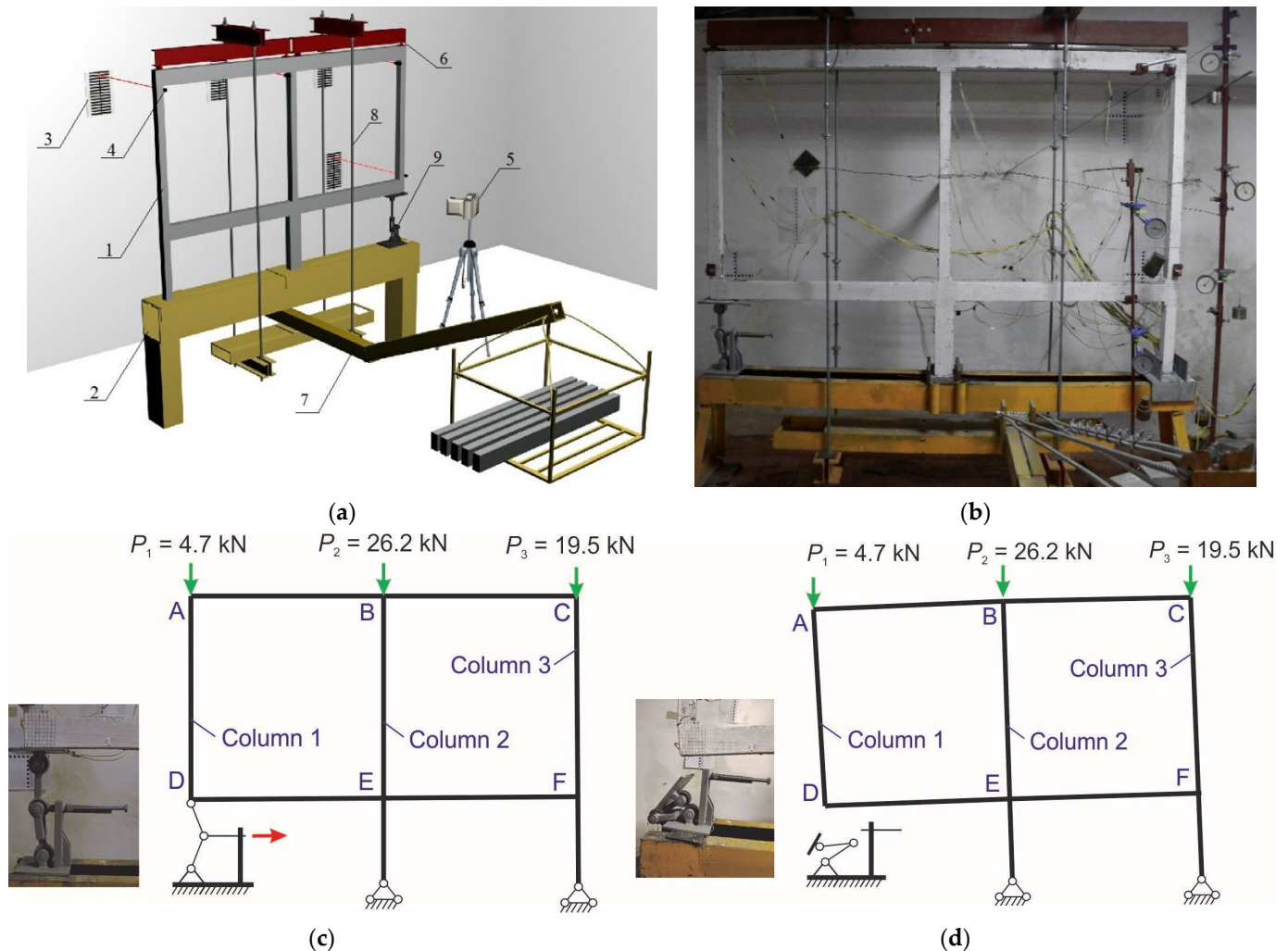


Figure 4. Test bench scheme (a); general view of the test bench (b); design scheme of the reinforced concrete frame in the first (c) and second stages of testing (d): 1—scaled reinforced concrete frame; 2—power frame; 3—graduated scale; 4—laser pointer; 5—video camera; 6—distribution beam; 7—leverage; 8—strands; 9—the device used to simulate the corner column.

The scheme and a view of the tie are presented in Figure 5a,b, respectively.

The method of testing the reinforced concrete frame consisted of two stages. In stage one, gravitational load was applied stepwise (10 steps) to upper joints A, B, and C of the experimental model using the leverage system shown in Figure 4c. Stability failure is associated with the action of a substantial axial load on a structure. Therefore, the frame was loaded using concentrated forces applied to the upper nodes of the specimen with an eccentricity of 5 mm in the cross direction. For simplicity, the beams of the frame were not loaded. However, the diagrams of moments in the beams of the specimen were similar to those in a real building frame with a corner column collapse. The difference between values of concentrated loads applied to the upper nodes of the frame is due to differences in slab loading areas and the anticipated effects of load transfer in the spatial building frame. The experiment also allowed for study of the load transfer between elements of a statically

indeterminate structure. Various loading options can also be numerically studied in the future using numerical models validated by the experimental data presented in this paper.

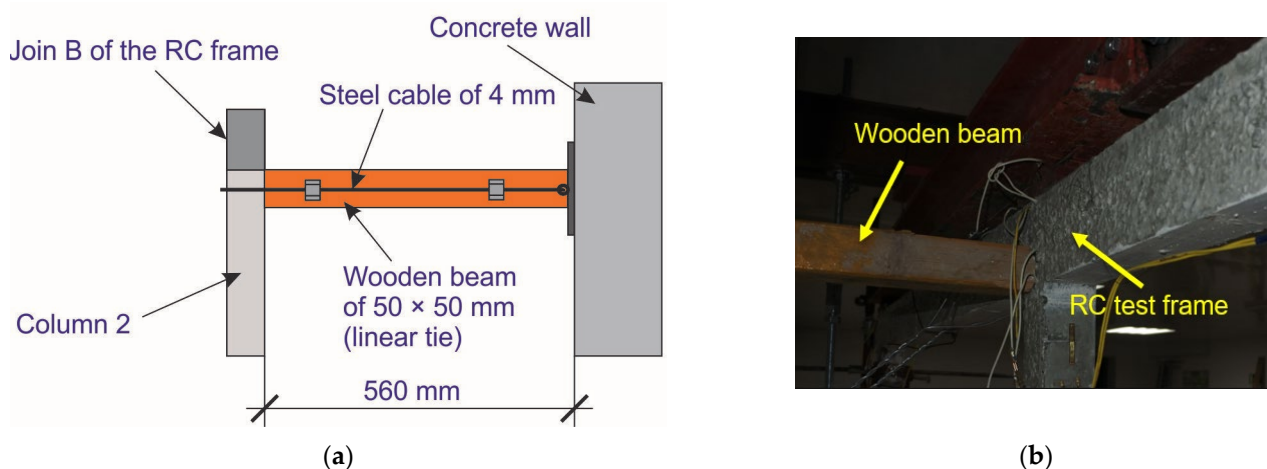


Figure 5. The scheme (a) and a general view (b) of linear ties fixing joint B in the cross direction of the test frame.

The instantaneous removal of a corner column located on the ground floor was simulated in the second stage. The column was removed by a special device [55] presented in Figure 4c. This device was instantly transformed into a mechanism when the second stage of testing was initiated, as shown in Figure 4d. The boundary conditions of joint D of the experimental frame were accepted as a simple support to simplify the physical modeling procedure. Hence, the experimental model did not take into account the bending moment, arising in the corner column of a real building frame before an accidental impact.

Laser pointers installed in the frame joints allowed for plotting of the displacement history in the second stage of testing when a special device simulated the sudden removal of the first-floor corner column. A video camera captured a video recording at a rate of up to 240 frames per second. Tracker freeware [56] was used to process the video.

3. Results

3.1. Experimental Results

3.1.1. Load–Displacement Curves in the First Stage of Physical Modeling

In accordance with the accepted testing method, the experimental frame was loaded using concentrated unequal forces during 10 stages as presented in Figure 4c. Figure 6a shows the loading graph for each upper joint of the frame. During the first stage of physical simulation, loads at joints A, B, and C of the frame and displacements at the points highlighted in yellow in Figure 6b were controlled. Load–displacement curves for the frame joints are presented in Figure 7a,b.

Displacement of the frame joints in the Y direction was due to the load transfer by the frame beams. Displacements along the X axis indicate the presence of initial eccentricities of applied concentrated forces in the X direction. Hence, uneven loading of building frames can lead to the emergence of additional geometric imperfections and stress concentrations in structural elements. In this experiment, such effects were small in quantitative terms due to the short duration of loading. However, they can trigger more pronounced changes in the stress–strain state of structures in the case of long-term loading. Therefore, they should be considered when the resistance of a building to accidental actions, such as a sudden collapse of a structural element, is analyzed.

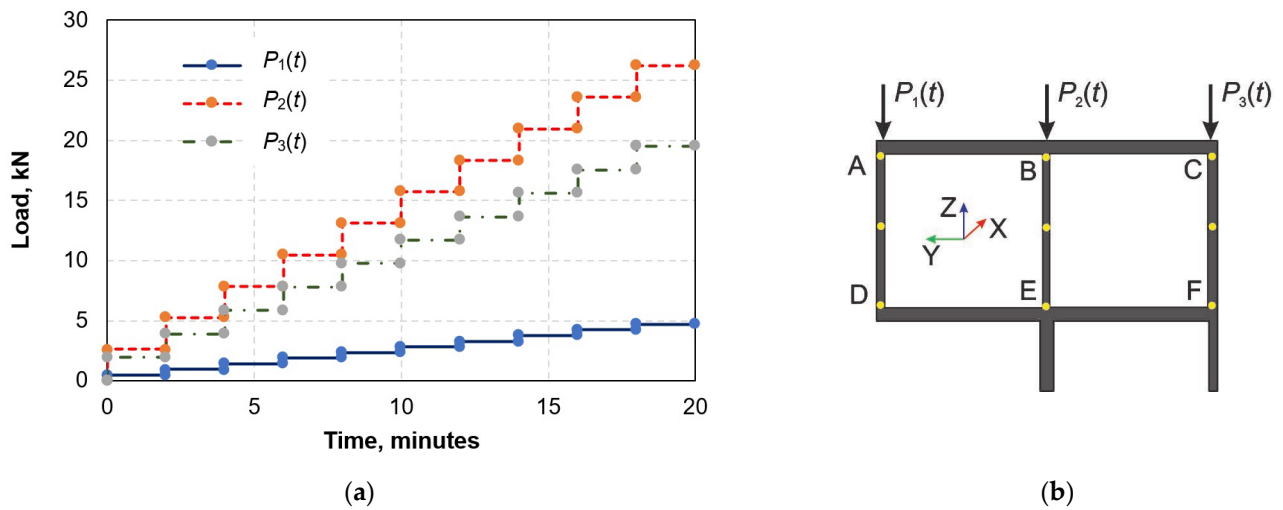


Figure 6. Loading graph for upper joints of the frame in the first stage of simulation (a) and displacement control points (b).

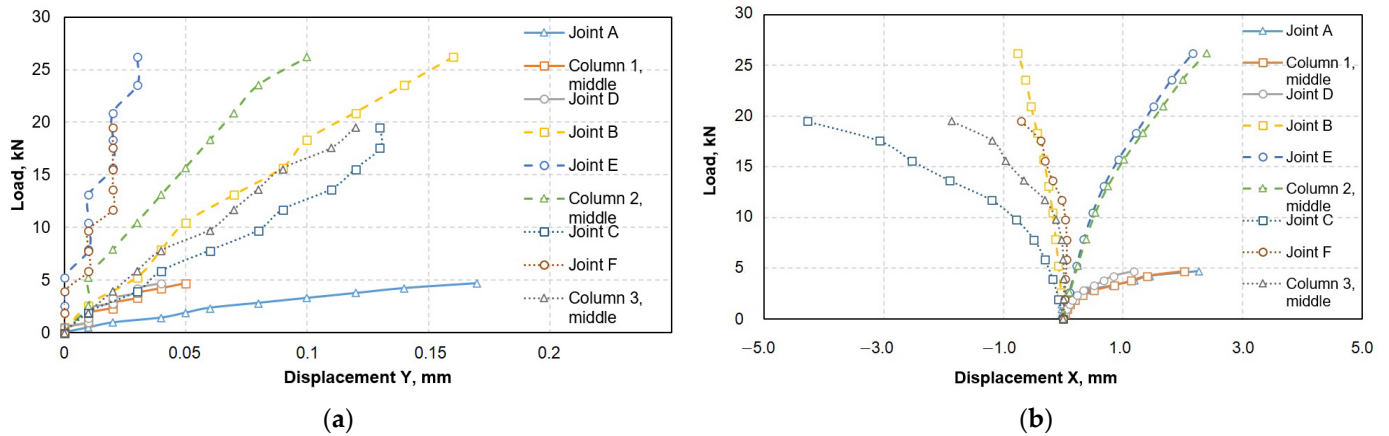


Figure 7. Horizontal displacement of the frame joints in the X (a) and Y (b) directions.

3.1.2. Dynamic Response of the Frame

Pursuant to the method described in Section 2, a simulation of the accidental impact on the reinforced concrete frame was performed. The contact between the device simulating the column removal and the joint of the experimental frame ceased 0.133 s after the triggering of the device (Figure 8). Furthermore, displacement Z of joint D reached its maximum value of 35 mm within the time range of 0.133 to 0.167 s. Displacement of joint D increased sharply after $t = 0.83$ s and converted into failure of the second-floor middle column (2) 1.167 s after removal of the corner column.

Video processing allowed for plotting of the vertical displacement of the beam-to-column joint after the accidental action was applied to the test frame, as presented in Figure 9a. Figures 9b and 10a show the Y and X horizontal displacement curves of joint C after the accidental impact on the experimental frame. Figure 10b shows the history of the X displacement of the section in the middle part of column 2 following the simulation of corner column removal.

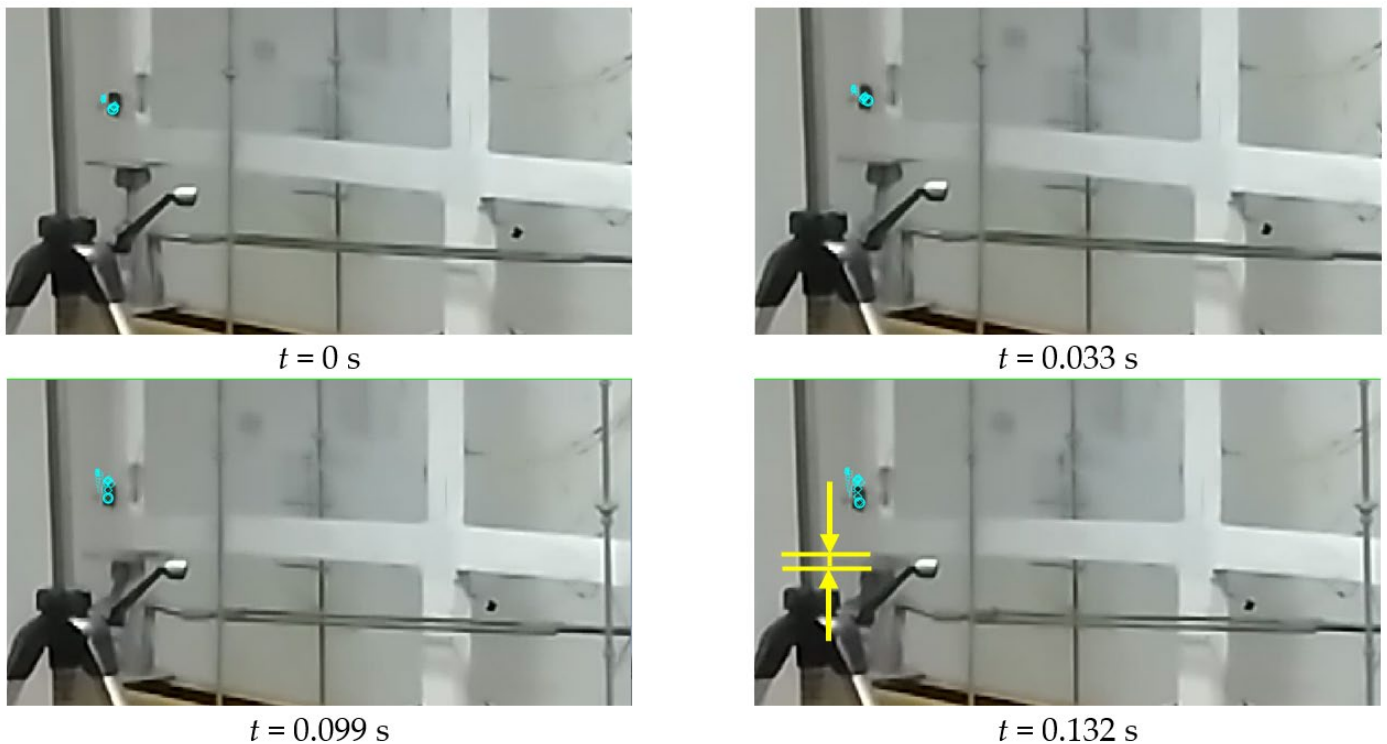


Figure 8. Displacement of the beam-to-column joint after removal of the corner column.

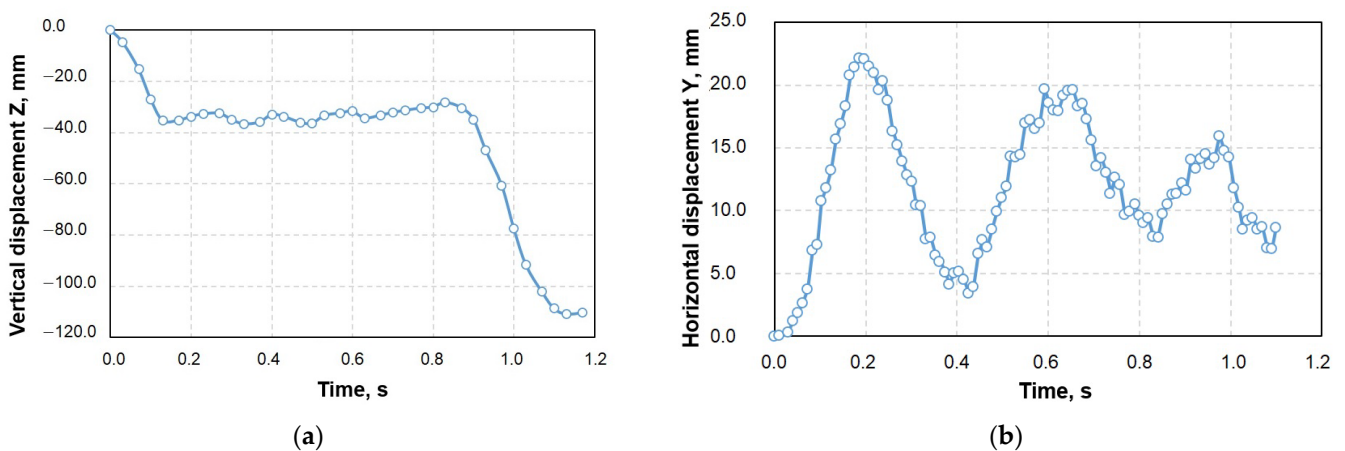


Figure 9. Displacement history of joint D for the Z direction (a) and of joint C for the Y direction (b).

Initial displacements of the frame caused by the loading in the first stage of the test were not considered in these curves. Analysis of curves allows for identification of the following features. First, the frame oscillated in the self-plane in the direction triggered by the response of the collapsed column (or support, as in the experiment), as presented in Figure 9a,b. However, the vibration mode became spatial after 0.3–0.5 s, as shown in Figure 10a,b. This was due to the dynamic properties of the structure and loading eccentricities.

3.1.3. Deformation and Failure of the Test Frame under a Corner Column Removal Scenario

Figures 11 and 12 show the side view of the deformation and failure of the tested reinforced concrete frame when the device simulating corner column removal became a mechanism.

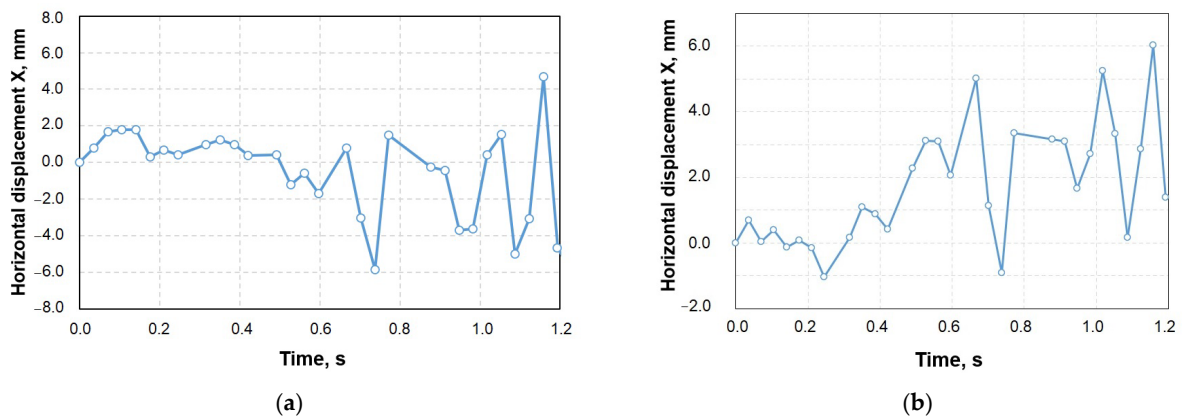


Figure 10. Displacement history of joint C for the X direction (a) and displacement history of the middle part of column 2 for the X direction (b).



Figure 11. Video processing data for deformation and failure of the test frame under the corner column removal scenario.

Video processing data show that the stability failure mechanism was triggered for column 2 within the time range of 1.134 to 1.167 s after removal of the corner column. This process was accompanied by a rapid increase in the out-of-plane lateral displacement of the test frame, which is typical for stability failure. Then, compressed concrete in the middle of the column height was destroyed within the time range of 1.167 to 1.2 s. After that, longitudinal steel reinforcement of the column buckled within the time range of $t = 1.2 \dots 1.233$ s (Figure 12f, and shear failure of the column was observed at the bottom end (E) (Figure 12e). Furthermore, torsion failure and 3D cracking occurred in upper beam-to-column joints A and C of the frame (Figure 12a,c). A wide crack opening was registered in joint E, as shown in Figure 11h, within the time range of 1.287 to 1.32 s. This process was accompanied by an increase in the beam rotation angle and destruction of test frame joint D presented (Figure 11g) at time $t = 1.353$ s.

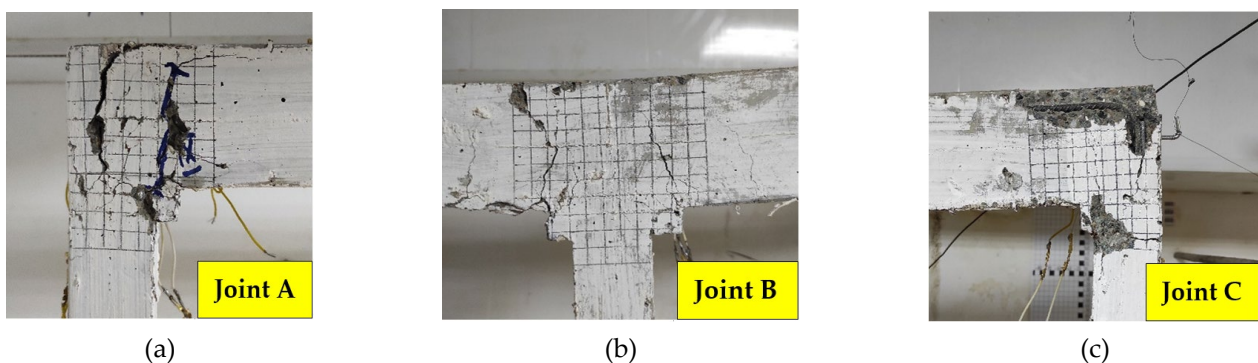


Figure 12. Cont.

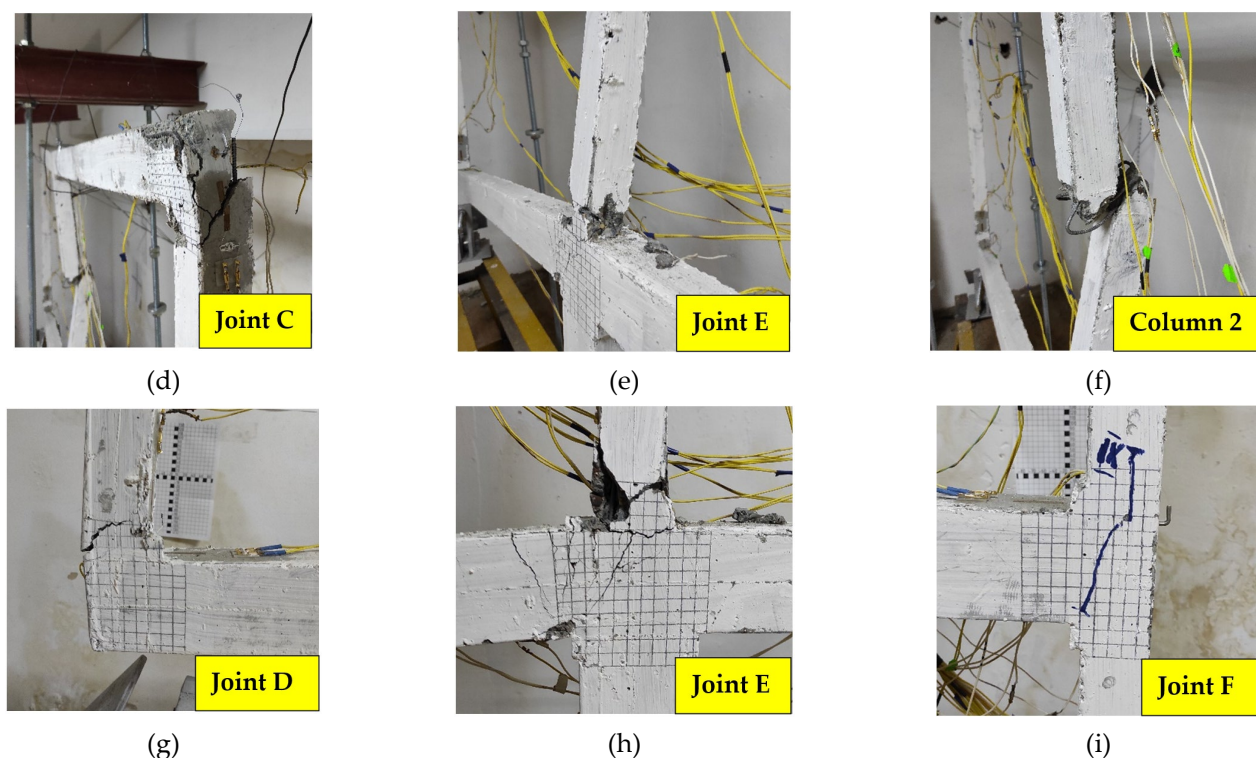


Figure 12. Test frame joints after an accidental impact: joint A front view (a), joint B front view (b), joint C front view (c), joint C side view (d), joint E side view (e), middle section of the column 2 (f), joint D front view (g), joint E front view (h), joint F front view (i).

3.2. Numerical Simulation Results

3.2.1. Finite Element Modeling and Criteria Used to Evaluate the Ultimate State of the Test Frame

To obtain detailed data on the resistance of the experimental reinforced concrete frame under the corner column removal scenario, a numerical study was performed using Ls-dyna software. Below, we present the finite element method equation used to solve the preset problem (1):

$$[M]\{u''\} + [C]\{u'\} + [K]\{u\} = \sum\{F\}, \quad (1)$$

where $\{u\}$, $\{u'\}$, and $\{u''\}$ are vectors of displacements, velocities, and accelerations in the nodes of the finite element model, respectively; $[M]$, $[C]$, and $[K]$ are mass, damping, and stiffness matrices, respectively; and $\sum\{F\}$ is the external load vector in the nodes of the finite element model. The explicit finite element method (FEM) was used to solve the problem.

The numerical model was developed in full compliance with the test frame presented in Figure 1. Figure 13 shows the resulting finite element model. This model was validated by comparing numerical and experimental curves of displacement histories.

Since simulation was performed according to the assumption of physical nonlinearity, the Euler critical force criterion could not be applied. Therefore, evaluation of the special limiting state (the ultimate state under progressive collapse) of structural elements and the frame was based on the tangent stiffness criterion, which assumes that the ultimate state satisfies condition (2):

$$dP/df = 0, \text{ and } M_{int} = M_{ext}, \quad (2)$$

where dP is the increment of axial loading of the element, df is the increment of lateral displacement, M_{int} is the internal moment in the section, and M_{ext} is the external moment caused by the loading.

In Formula (2), the first condition demonstrates the violation of proportionality between the impacts and the structure's response. The second condition is the condition

of structural integrity of the element. Otherwise, there is no force equilibrium in a cross section.

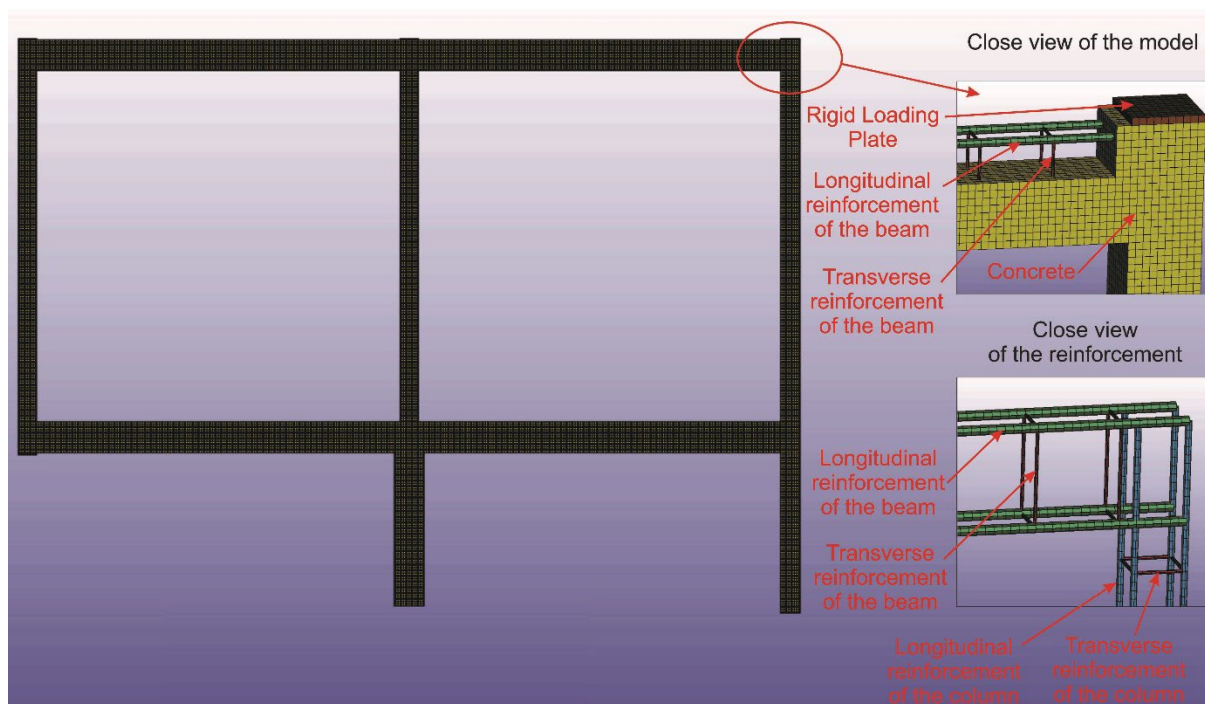


Figure 13. Finite element model of the test frame developed using Ls-dyna software.

3.2.2. Finite Element Types

The concrete part of the reinforced concrete frame was simulated using eight-node solid finite elements (solid 164) and the preset ELFORM = 2 property. A mesh size of 5 mm was adopted for solid finite elements based on the mesh sensitivity analysis.

The reinforcement was simulated using two-node beam-type elements. The mesh size of these elements was the same as that of concrete elements (5 mm). The contact was assumed to be perfect between reinforcement bars and concrete. Since the process of crack opening and closing changed over time, simulation of an imperfect contact would be a complex problem.

3.2.3. Loads and Boundary Conditions

To simulate the boundary conditions arising between the frame and the test bench, special plates were simulated using eight-node finite elements. The absolutely rigid material model *Mat_Rigid was applied to these plates to prevent any additional stress concentration in areas of concentrated responses. Perfect contact without friction was assumed between the plate and the reinforced concrete frame using the keyword *Contact_Automatic_Surface_To_Surface (*CASTS).

Linear ties (presented in Figure 5a) were simulated by fixing corresponding nodes of the finite element model in the X direction.

The load applied to the upper nodes of the frame was transferred through the plates. This load was transferred in the form of concentrated forces similar to those mentioned above. Concentrated forces were applied to the plates with an eccentricity of 5 mm in the negative direction of the X axis. This eccentricity allowed for simulation of perturbation arising from the frame plane. In real structures of reinforced concrete frames of buildings, such an eccentricity can arise in columns under the combined action of an axial force and a bending moment. In this regard, consideration of eccentricities is allowable in the course of testing and conducting numerical simulations.

The first stage of the quasistatic loading of the frame specimen was simulated in Ls-dyna by applying loads for $t_1 = 0.05$ s according to the scheme presented in Figure 4c. To exclude the dynamic effects on the structure during this loading stage, command *Control_Dynamic_Relaxation was applied in Ls-dyna. The DRFCTR factor was set to a default value of 0.995. In the second stage, the rigid plate under joint D of the frame was subjected to a displacement of $w_0 = 1$ m in the negative direction of the Z axis for the time $t_2 - t_1 = 0.1$ s in accordance with the experimental data. The integration time was accepted as $t_3 = 1.3$ s with an integration step of 0.0005 s. Figure 14 presents the numerical simulation scheme for the loading process.

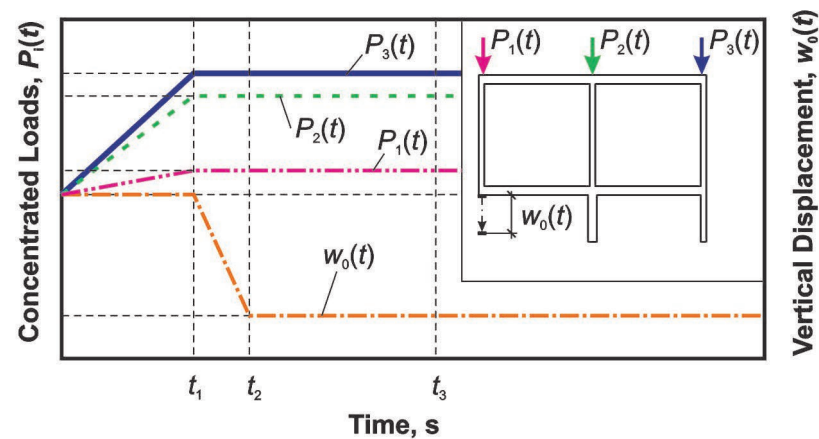


Figure 14. The loading process within the framework of the numerical simulation.

3.2.4. Material Modeling

A continuous surface cap model (CSCM) [57] was applied to simulate the material properties of concrete in the numerical simulation. The following CSCM parameter values were set: RO = 2.324×10^{-9} ton/mm³ (mass density); ERODE: 1.05 (the option to erode with strain at which erosion initiates); FPC: 25.2 MPa (concrete compressive strength). The model of the isotropic elastic–plastic material *Mat_Piecewise_Linear_Plasticity was applied to simulate the steel reinforcement. The following input parameters were adopted for this model: RO: 7.85×10^{-9} ton/mm³ (mass density); E: 2×10^5 MPa (elasticity modulus); PR: 0.3 (Poisson’s ratio); ETAN: 10 MPa (tangent modulus); yielding strength of steel reinforcement A500 SIGY: 606.4 MPa; the same for Bp500 SIGY: 526.5 MPa, as well as for A240 SIGY: 317.1 MPa. Figure 15a shows the CSCM yield surface for concrete. The stress–strain diagrams accepted for the steel reinforcement are presented in Figure 15b.

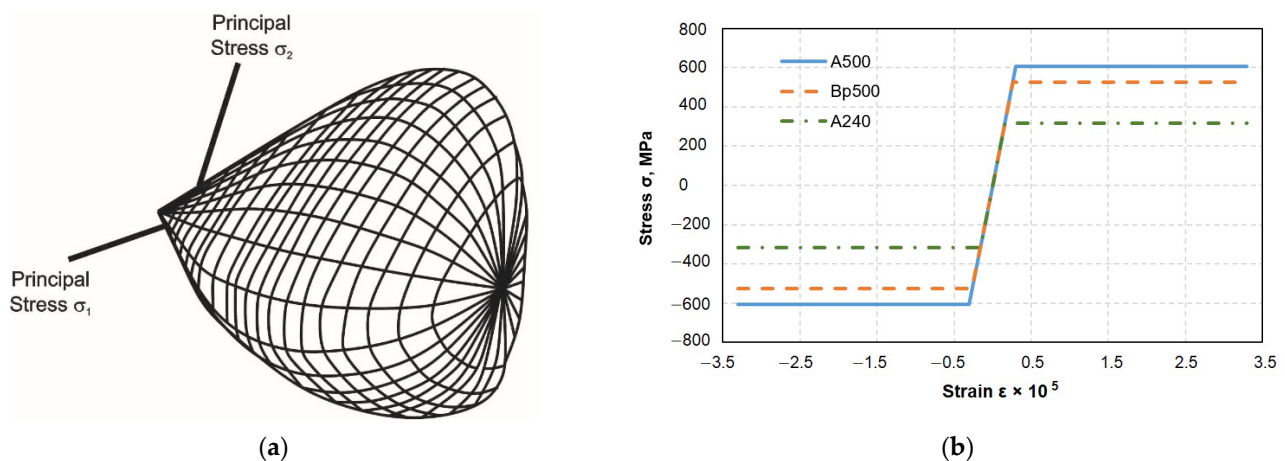


Figure 15. Material models accepted for numerical simulation: CSCM yield surface for concrete (a); piecewise linear diagrams for the steel reinforcement (b).

3.2.5. Comparison between the Experimental Results and Numerical Simulation

Figure 16 shows the history of displacements for (1) structural joint D and (2) a section in the middle part of column 2, where stability failure was identified in the experiment.

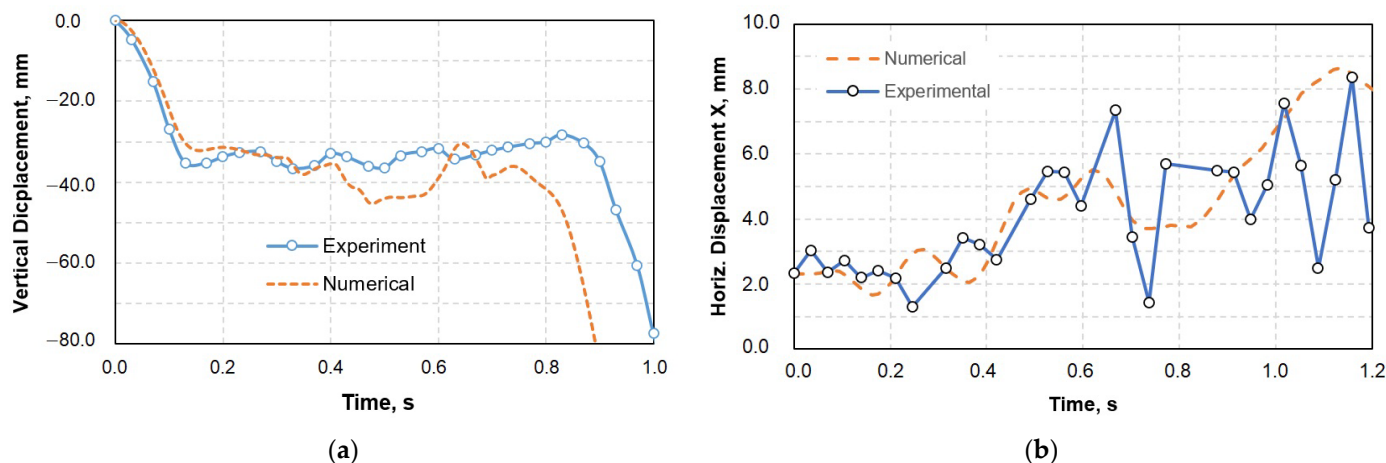


Figure 16. The history of displacements for structural joint D in the direction of the Z axis (a) and a section in the middle part of column 2 in the direction of the X axis (b).

The numerical curve of the history of vertical displacement of joint D reproduces the experimental curve up to time point 0.4 s after the accidental impact on the frame (corner column removal). Starting from 0.4 s, there was a discrepancy between the simulation and the experiment data, which reached 34%. The discrepancy (Figure 16b) is due to the influence of (1) natural vibrations of the loading device on experimental results and (2) cracking of the experimental frame before the collapse of column 2. However, experimental and numerical results remain close with respect to the maximum values of column displacements before the collapse. The simulated X displacement of the middle part of column 2 at the moment of destruction practically coincided with the experimental data, with values of 8.64 and 8.43 mm, respectively.

The damage patterns, as well as the deformed state of the frame (Figure 17), simulated in Ls-dyna almost coincide with the test data presented in Figure 11. Large openings of cracks in frame joints A, B, D, and E were observed in the course of simulation. Destruction of compressed concrete was observed in the middle part of column 2. In joints C and F and the bottom section of column 2 (joint E), values of effective plastic strain were particularly high, which indicates cracking in these areas. Figure 18 shows the deformed state of the steel bars of the frame reinforcing cages and the axial forces acting in them at the moment of the column 2 collapse. Steel bars of the longitudinal reinforcement of column 2 are buckled in the middle part of the structure, which coincides with the experimental data presented in Figure 12f. At the beginning of compressed concrete destruction in the middle part of column 2, forces did not exceed the yield strength of steel in any of the reinforcing bars.

Some features of destruction of the experimental frame, such as the deformed state and the damaged area, were triggered by a combination of actual boundary conditions and the loading pattern. However, the above-mentioned mechanism of destruction associated with stability failure can potentially be implemented in the frames of buildings with slender columns in the case of an extreme situation in which an accidental impact on a structure leads to a substantial increase in an axial force and a bending moment.

Failure mechanisms of a reinforced concrete frame with slender columns can be classified as a combination of a pancake type and a domino type of progressive collapse according to Kiakojoury et al. with due regard to the results of physical and numerical simulations [11].

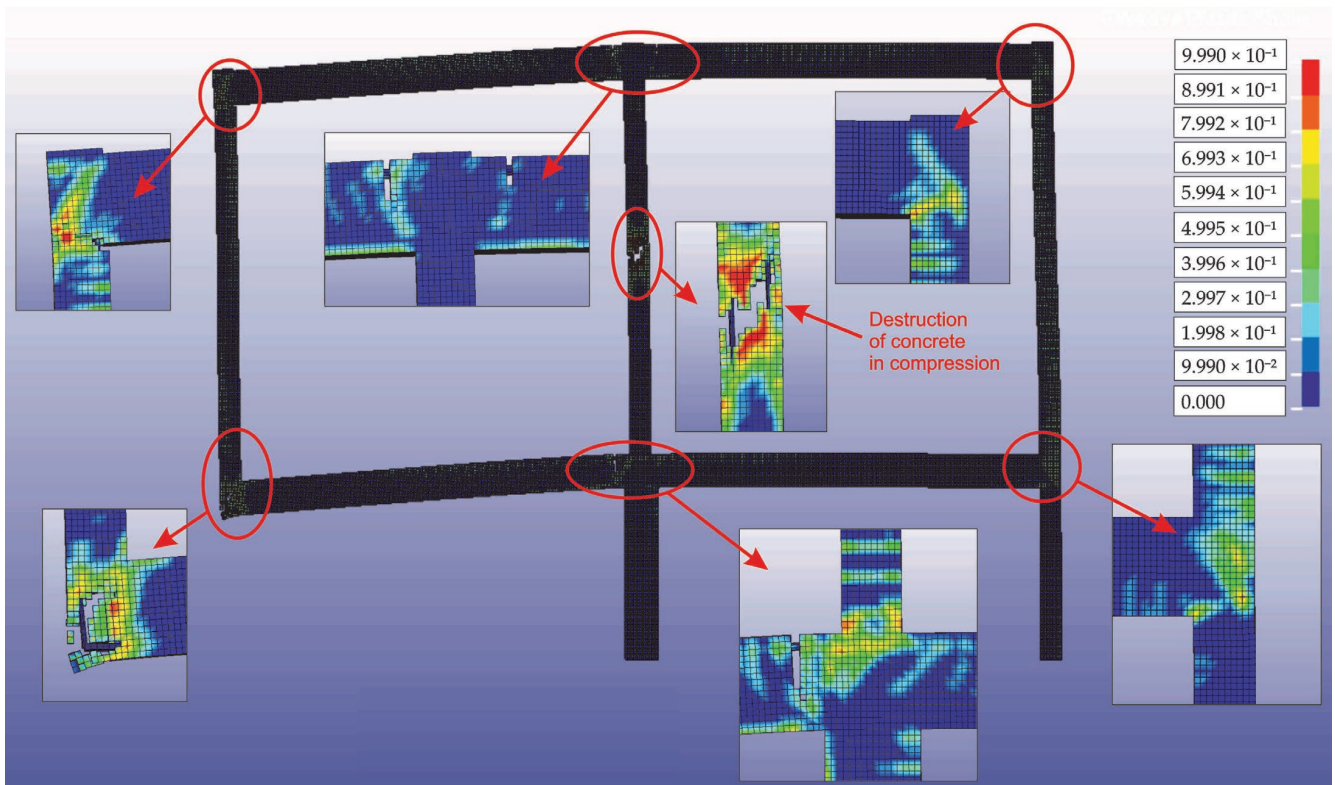


Figure 17. Effective plastic strain in the specimen.

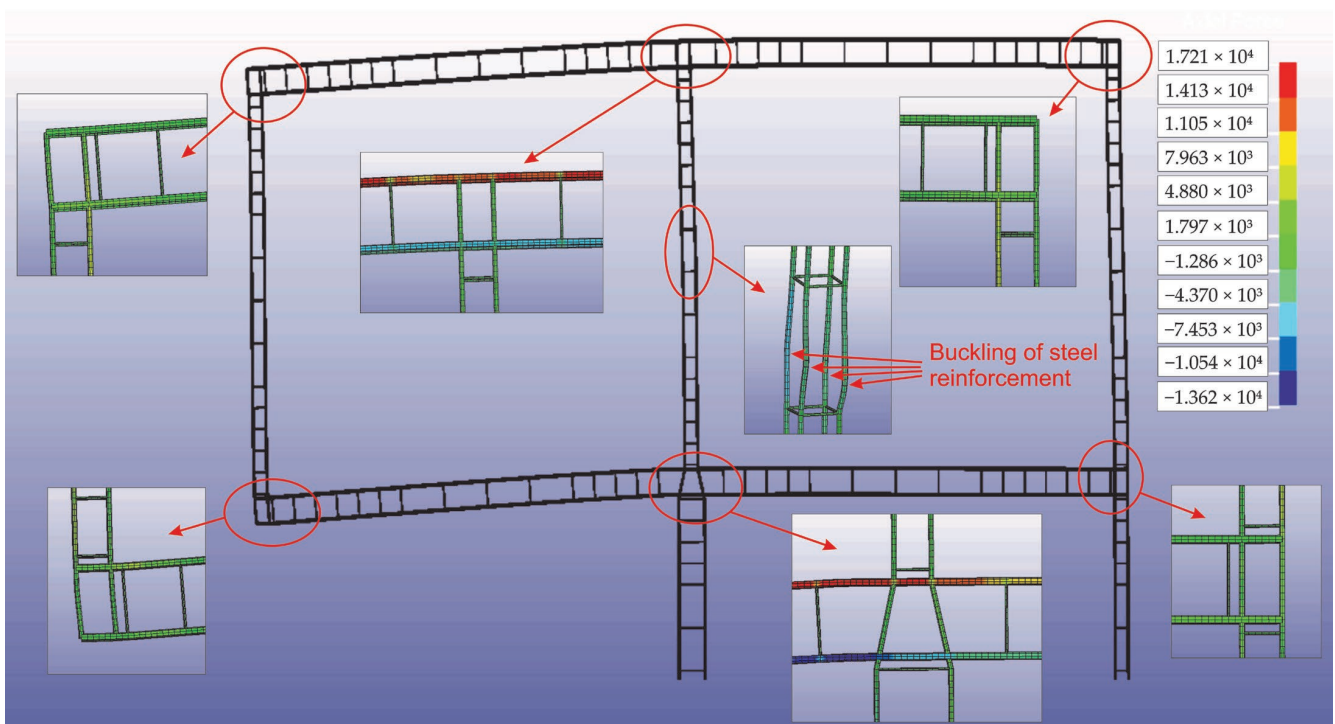


Figure 18. Axial forces in the steel reinforcement bars of the frame, N .

3.2.6. Analysis of the Failure Mechanism and the Criterion of Tangent Stiffness

Figures 19 and 20 show graphs of the force–displacement relations for the characteristic joints of the frame. For the middle of column 2, where the stability failure mechanism was observed experimentally, an extremum was observed on the force–displacement graph

(Figure 19a) at the moment of reaching the peak axial force over time (Figure 19b). This means that when the axial force reaches the peak value of 25.95 kN, the tangential stiffness of the column is null. After that, the secondary redistribution of forces from column 2 to other elements of the frame occurred. Further deformation of column 2 was determined by the tangential stiffness of the frame in the direction of the axial force action in the destroyed element. Physically, this process was accompanied by the destruction of the sections of column 2, as presented in Figure 19c, which shows the state of the finite element model at the moment of reaching the peak value of the axial force in column 2.

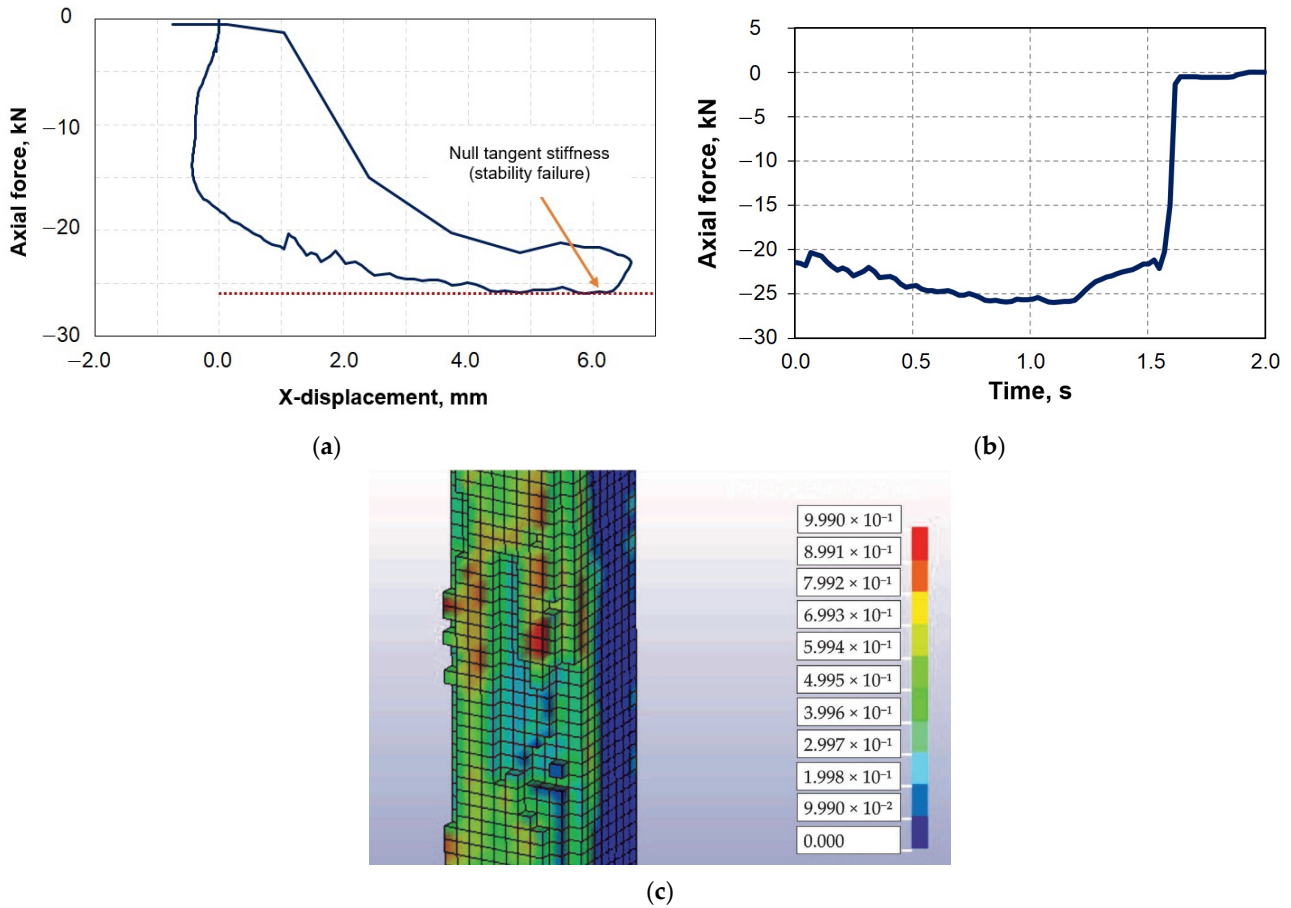


Figure 19. The axial force–X displacement curve (a), history of axial force (b), and effective plastic strain when tangent stiffness is null (c) for a section in the middle part of column 2.

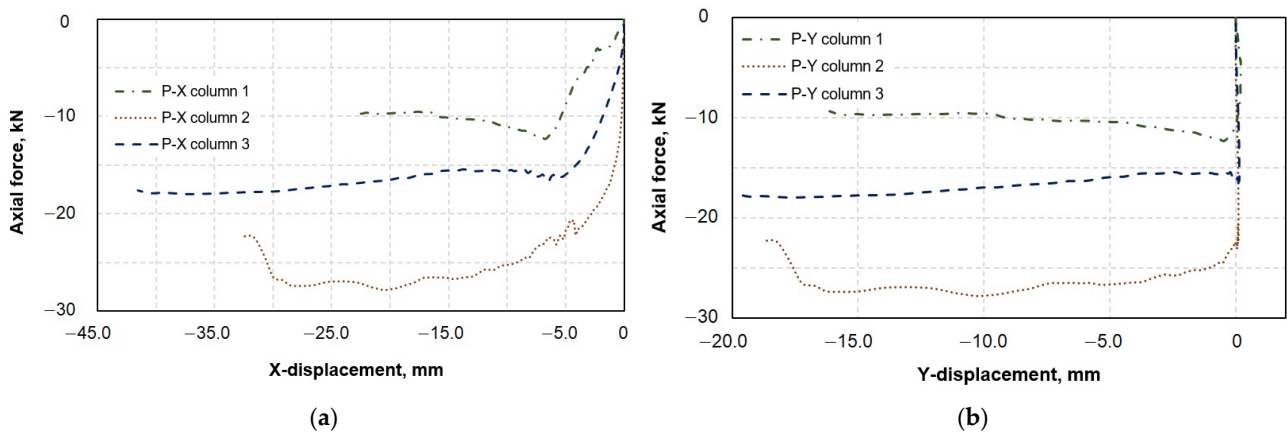


Figure 20. Force–displacement curves for the top edges of the columns: axial force–X displacement curve (a) and axial force–Y displacement curve (b).

Similar relations were also observed in the top section of column 2, in which the physical process of destruction did not occur. The achievement of the peak value of the axial force was replaced by an increase in X and Y displacements and a reduction in forces in the top sections of column 2 (Figure 20a,b). There were no such extrema in columns 1 and 3. After the initial quasistatic stage of loading, insignificant deloading occurred, which was caused by the redistribution of forces that followed alternative loading paths. Then, a minor increase in forces was observed in these load-bearing elements. This process was accompanied by an increase in displacements in X and Y directions. Thus, the criterion of tangent stiffness can be applied to evaluate not only the strength of the section but also the bearing capacity of the elements and the frame.

4. Conclusions

In this paper, we present the results of experimental and numerical studies of the structural behavior and failure of a scale reinforced concrete frame with slender columns under a sudden corner column removal scenario. For the purposes of this study, a physical model of a reinforced concrete frame of a multistory building was proposed using the theory of functional similarity. A finite element model was developed for the numerical study that was exactly the same as the tested frame. We validated this model by comparing the numerical and experimental curves of displacement histories. Based on the simulation and experimental data, the dynamics of the frame under an accidental impact, the failure mechanism, and the relationship between the forces (stresses) and displacements in structural elements were studied. The following main conclusions were made on the basis of the results of this study:

1. Experimental and numerical studies of the behavior of a reinforced concrete frame under quasistatic loading with concentrated unequal loads revealed the load transfer between columns through the beams. Although these effects were minor in the frame under consideration due to the short loading period, their effect can be more significant under long-term loading. Therefore, they should be considered when the resistance of a building to accidental actions, such as a sudden collapse of a structural element, is analyzed.
2. The failure mechanism of the reinforced concrete frame under consideration was triggered by the loss of stability of the column. The failure was fragile. No more than 0.033 s passed from the moment when the first signs of damage were detected to the complete destruction of compressed concrete in the middle part of the column. Some features of destruction of the experimental frame, such as the deformed state and patterns of damages, were, to a large extent, caused by a combination of actual boundary conditions and the loading pattern. However, stability failure can potentially be implemented in the frames of buildings with slender columns in the case of an extraordinary situation in which an accidental impact on a structure leads to a substantial increase in an axial force and a bending moment.
3. The moment of the stability failure of the column of the experimental frame corresponded to the extremum on the force–displacement curve, indicating null tangent stiffness. Thus, the criterion of tangent stiffness can be proposed to evaluate the ultimate state of a structure subjected to an accidental impact.

Author Contributions: This study was designed, directed, and coordinated by S.S., V.K. and N.F.; S.S., V.K. and N.F. planned and performed an experimental investigation of RC frame stability failure under a corner column removal scenario. S.S., V.K., N.F. and N.T.V. planned and performed the numerical study of RC frame stability failure under a corner column removal scenario and analyzed the resulting data. The manuscript was written by S.S., V.K., N.F. and N.T.V. All authors have read and agreed to the published version of the manuscript.

Funding: This research received no external funding.

Institutional Review Board Statement: Not applicable.

Informed Consent Statement: Not applicable.

Data Availability Statement: The data presented in this research are available and can be obtained from the corresponding author upon request.

Conflicts of Interest: The authors declare no conflict of interest.

References

1. Wang, H.; Zhang, A.; Li, Y.; Yan, W. A Review on Progressive Collapse of Building Structures. *Open Civ. Eng. J.* **2014**, *8*, 183–192. [CrossRef]
2. Abdelwahed, B. A Review on Building Progressive Collapse, Survey and Discussion. *Case Stud. Constr. Mater.* **2019**, *11*, e00264. [CrossRef]
3. Fedorova, N.V.; Savin, S.Y. Progressive Collapse Resistance of Facilities Experienced to Localized Structural Damage—An Analytical Review. *Build. Reconstr.* **2021**, *95*, 76–108. [CrossRef]
4. Ellingwood, B.R.; Smilowitz, R.; Dusenberry, D.O.; Duthinh, D.; Lew, H.S.; Carino, N.J. *Best Practices for Reducing the Potential for Progressive Collapse in Buildings*; U.S. National Institute of Standards and Technology (NIST): Gaithersburg, MD, USA, 2007. Available online: <https://www.nist.gov/publications/best-practices-reducing-potential-progressive-collapse-buildings> (accessed on 21 November 2022).
5. Tamrazyan, A.G.; Alekseytsev, A.V. Optimization of Reinforced Concrete Beams under Local Mechanical and Corrosive Damage. In *Engineering Optimization*; Taylor & Francis: Oxford, UK, 2022.
6. Alekseytsev, A.V. Mechanical Safety of Reinforced Concrete Frames under Complex Emergency Actions. *Mag. Civ. Eng.* **2021**, *103*, 10306.
7. Pearson, C.; Delatte, N. Ronan Point Apartment Tower Collapse and its Effect on Building Codes. *J. Perform. Constr. Facil.* **2005**, *19*, 172–177. [CrossRef]
8. Kong, X.; Smyl, D. Investigation of the Condominium Building Collapse in Surfside, Florida: A Video Feature Tracking Approach. *Structures* **2022**, *43*, 533–545. [CrossRef]
9. Tagel-Din, H.; Rahman, N.A. Simulation of the Alfred P. Murrah Federal Building Collapse due to Blast Loads. In Proceedings of the AEI 2006: Building Integration Solutions, Proceedings of the 2006 Architectural Engineering National Conference, Omaha, NE, USA, 29 March–1 April 2006.
10. Belostotsky, A.M.; Pavlov, A.S. Long Span Buildings Analysis under Physical, Geometric and Structural Nonlinearities Consideration. *Int. J. Comput. Civ. Struct. Eng.* **2010**, *6*, 80–86.
11. Kiakojour, F.; Biagi, V.D.; Chia, B.; Sheidaii, M.R. Progressive collapse of framed building structures: Current knowledge and future prospects. *Eng. Struct.* **2020**, *206*, 110061. [CrossRef]
12. *UFC 4-023-03; Design of Buildings to Resist Progressive Collapse. Unified Facilities Criteria; Department of Defense (DoD): Washington, DC, USA, 2016.* Available online: https://wbdg.org/FFC/DOD/UFC/ufc_4_023_03_2009_c3.pdf (accessed on 21 November 2022).
13. General Services Administration (GSA). *Alternative Path Analysis and Design Guidelines for Progressive Collapse Resistance*; Office of Chief Architects: Washington, DC, USA, 2013. Available online: https://www.gsa.gov/cdnstatic/Progressive_Collapse_2016.pdf (accessed on 21 November 2022).
14. *ASCE/SEI 7-16; Minimum Design Loads and Associated Criteria for Buildings and Other Structures.* Structural Engineering Institute of the ASCE; American Society of Civil Engineers (ASCE): Reston, VA, USA, 2016. Available online: <https://law.resource.org/pub/us/cfr/ibr/003/asce.7.2002.pdf> (accessed on 21 December 2022).
15. *EN 1991-1-7; Eurocode 1—Actions on Structures—Part 1-7: General Actions—Accidental Actions.* CEN Comité Européen de Normalisation CEN: Brussels, Belgium, 2006. Available online: <https://www.phd.eng.br/wp-content/uploads/2015/12/en.1991.1.7.2006.pdf> (accessed on 21 November 2022).
16. *GOST 27751-2014; Reliability for Constructions and Foundations. General Principles.* National Standard of Russian Federation; JSC Research Center “Construction”: Moscow, Russia, 2019. Available online: <https://docs.cntd.ru/document/1200115736> (accessed on 21 November 2022).
17. *SP 385.1325800.2018; Protection of Buildings and Structures against Progressive Collapse. Design Code. Basic Statements;* National Building Code of Russian Federation; Ministry of Construction, Housing and Utilities: Moscow, Russia, 2018. Available online: <https://docs.cntd.ru/document/551394640> (accessed on 21 November 2022).
18. Bažant, Z.P.; Verdure, M. Mechanics of Progressive Collapse: Learning from World Trade Center and Building Demolitions. *J. Eng. Mech.* **2007**, *133*, 308–319. [CrossRef]
19. Kwasniewski, L. Nonlinear Dynamic Simulations of Progressive Collapse for a Multistory Building. *Eng. Struct.* **2010**, *32*, 1223–1235. [CrossRef]
20. Yousef, A.M.; El-Mandouh, M.A. Dynamic Analysis of High-Strength Concrete Frame Buildings for Progressive Collapse. *Case Stud. Constr. Mater.* **2020**, *13*, e00470. [CrossRef]
21. Almazov, V.O.; Plotnikov, A.I.; Rastorguev, B.S. Problems of Buildings Resistance to Progressive Collapse. *Vestn. MGSU* **2011**, *2–1*, 16–20.

22. Kabantsev, O.; Mitrovic, B. Deformation and Power Characteristics Monolithic Reinforced Concrete Bearing Systems in the Mode of Progressive Collapse. *MATEC Web Conf.* **2018**, *251*, 02047. [CrossRef]
23. Mohamed, O.A.; Keshawarz, M.S. Modeling for Progressive Collapse Mitigation Using Nonlinear Static Analysis Procedures. In Proceedings of the CST 2008, the Ninth International Conference on Computational Structures Technology, Athens, Greece, 2–5 September 2008.
24. Kodysch, E.N.; Trekin, N.N.; Chesnokov, D.A. Protection of Multistory Buildings from progressing collapse. *PromyshlennoeiGrazhdanskoe Stroit.* **2016**, *6*, 8–13. Available online: <http://www.pgs1923.ru/ru/index.php?m=4&y=2016&v=06&p=00&r=02> (accessed on 21 November 2022).
25. Adam, J.M.; Parisi, F.; Sagaseta, J.; Lu, X. Research and Practice on Progressive Collapse and Robustness of Building Structures in the 21st Century. *Eng. Struct.* **2018**, *173*, 122–149. [CrossRef]
26. Nazarov, Y.V.; Zhuk, Y.N.; Simbirkin, V.N.; Egorov, M.I. Basmany Market: Analysis of Design Solutions and Possible Mechanisms of Building Destruction. *Struct. Mech. Anal. Constr.* **2007**, *211*, 49–55.
27. Almusallam, T.; Al-Salloum, Y.; Elsanadedy, H.M.; Ngo, T.D.; Mendis, P.; Abbas, H. Development Limitations of Compressive Arch and Catenary Actions in Reinforced Concrete Special Moment Resisting Frames under Column-Loss Scenarios. *Struct. Infrastruct. Eng.* **2020**, *16*, 1616–1634. [CrossRef]
28. Shi, F.; Wang, L.; Dong, S. Progressive Collapse Assessment of the Steel Moment-frame with Composite Floor Slabs Based on Membrane Action and Energy Equilibrium. *Open Constr. Build. Technol. J.* **2017**, *11*, 200–215. [CrossRef]
29. Shan, L.; Petrone, F.; Kunnath, S. Robustness of RC Buildings to Progressive Collapse: Influence of Building Height. *Eng. Struct.* **2019**, *183*, 690–701. [CrossRef]
30. Sasani, M.; Sagioglu, S. Progressive Collapse Resistance of Hotel San Diego. *J. Struct. Eng.* **2008**, *134*, 478–488. [CrossRef]
31. Kolcunov, V.I.; Tuyen, V.N.; Korenkov, P.A. Deformation and Failure of a Monolithic Reinforced Concrete Frame under Accidental Actions. *IOP Conf. Ser. Mater. Sci. Eng.* **2020**, *753*, 032037.
32. Zheng, Y.; Xiong, J.; Wu, Z.; He, Y. Experimental Study on Progressive Collapse Resistance of Reinforced Concrete Frame Structures. *Appl. Mech. Mater.* **2011**, *71–78*, 871–875. [CrossRef]
33. Shan, S.; Li, S. Experimental Study on the Progressive Collapse Performance of RC Frames with Infill Walls. *Eng. Struct.* **2016**, *250*, 113451. [CrossRef]
34. Yang, T.; Chen, W.; Han, Z. Experimental Investigation of Progressive Collapse of Prestressed Concrete Frames after the Loss of Middle Column. *Adv. Civ. Eng.* **2020**, *2020*, 8219712. [CrossRef]
35. Fedorova, N.V.; Ngoc, V.T. Deformation criteria for reinforced concrete frames under accidental actions. *Mag. Civ. Eng.* **2022**, *109*, 10902.
36. Adam, J.M.; Buitrago, M.; Bertolesi, E.; Sagaseta, J.; Moragues, J.J. Dynamic Performance of a Real-Scale Reinforced Concrete Building Test under a Corner-Column Failure Scenario. *Eng. Struct.* **2020**, *210*, 110414. [CrossRef]
37. Tamrazyan, A.G.; Avetisyan, L.A. Experimental and Theoretical Study of Reinforced Concrete Elements under Different Characteristics of Loading at High Temperatures. *Procedia Eng.* **2016**, *153*, 721–725. [CrossRef]
38. Popov, D.S. Experimental Studies of Dynamic Properties of Corrosion-Damaged Compressed Reinforced Concrete Elements. *Build. Reconstr.* **2022**, *100*, 55–64. [CrossRef]
39. Savin, S.; Kolchunov, V.; Fedorova, N. Dynamic Response of a Reinforced Concrete Column under Axial Shock Impact. *Mech. Mach. Sci.* **2023**, *125*, 43–52.
40. Sanzharovskiy, R.S. *Stability of Elements of Building Structures during Creep*; Publishing of Leningrad University: Leningrad, Russia, 1984; 217p.
41. Golyshhev, A.B.; Kolchunov, V.I.I. *The Resistance of Reinforced Concrete*; Osnova: Kiev, Ukraine, 2009.
42. Gemmerling, A.V. *Bar Structural Systems Analysis*; Stroyizdat: Moscow, Russia, 1974; 207p.
43. Fedorova, N.V.; Savin, S.Y.; Kolchunov, V.I. Affecting of the Long-Term Deformation to the Stability of RC Frame-Bracing Structural Systems under Special Accidental Impacts. *IOP Conf. Ser. Mater. Sci. Eng.* **2020**, *753*, 032005. [CrossRef]
44. Savin, S.Y.; Kolchunov, V.I.; Korenkov, P.A. Experimental Research Methodology for the Deformation of RC Frame under Instantaneous Loss of Column. *IOP Conf. Ser. Mater. Sci. Eng.* **2020**, *962*, 022054. [CrossRef]
45. Geniyev, G.A. On Dynamic Effects in Rod Systems Made of Physical Non-Linear Brittle Materials. *PromyshlennoeiGrazhdanskoe Stroit.* **1999**, *9*, 23–24.
46. Kirpichev, M.V. *Theory of Similarity*; Publishing of Academy of Science of USSR: Moscow, Russia, 1953; 93p.
47. Sedov, L.I. *Similarity Methods and Dimensions in Mechanics*, 8th ed.; Nauka: Moscow, Russia, 1972; 440p.
48. Chemodurov, V.T.; Korenkov, P.A.; Leonenko, Y.S.; Korenkova, O.O. Physical Modeling of Reinforced Concrete Structures Exposed to Emergency Loads. *J. Phys. Conf. Ser.* **2020**, *1425*, 012061. [CrossRef]
49. Bazant, Z.P.; Kwon, Y.W. Failure of slender and stocky reinforced concrete columns: Tests of size effect. *Mater. Struct.* **1994**, *27*, 79–90. [CrossRef]
50. *ACI 318-19; Building Code Requirements for Structural Concrete and Commentary*. American Concrete Institute: Indianapolis, IN, USA, 2019; An ACI Standard. Available online: <https://www.concrete.org/publications/internationalconcreteabstractsportal.aspx?m=details&ID=51716937> (accessed on 21 March 2023).

51. SP 63.13330.2018; Concrete and Reinforced Concrete Structures. General Provisions. National Building Code of Russian Federation; Ministry of Construction, Housing and Utilities: Moscow, Russia, 2022. Available online: <https://docs.cntd.ru/document/554403082> (accessed on 21 March 2023).
52. Bezgodov, I.M. Relations of Strength and Deformation Characteristics of Concrete under Compression, Tension and Tension in Bending. *Beton i Zhelezobeton* **2012**, *2*, 2–5.
53. GOST 10180-2012; Concretes. Methods for Strength Determination Using Reference Specimens. National Standard of the Russian Federation; JSC Research Center “Construction”: Moscow, Russia, 2012. Available online: <https://docs.cntd.ru/document/1200100908> (accessed on 21 November 2022).
54. GOST 18105-2018; Concretes. Rules for Control and Assessment of Strength. National Standard of the Russian Federation; JSC Research Center “Construction”: Moscow, Russia, 2018. Available online: <https://www.mos.ru/upload/documents/files/2071/GOST18105-2018.pdf> (accessed on 21 November 2022).
55. Klyueva, N.V.; Korenkov, P.A. Device for Experimental Determination of Dynamic Addition Loading in Frame-Rod Structural Systems. Patent RU 2642542, 25 January 2018. Russian Federation p. 1. Available online: https://patents.s3.yandex.net/RU2642542C1_20180125.pdf (accessed on 21 November 2022).
56. Tracker. Video Analysis and Modeling Tool for Physics Education. Available online: https://physlets.org/tracker/change_log.html (accessed on 11 September 2021).
57. Users Manual for LS-DYNA Concrete Material Model 159. Available online: <https://www.fhwa.dot.gov/publications/research/infrastructure/pavements/05062/05062.pdf> (accessed on 8 December 2022).

Disclaimer/Publisher’s Note: The statements, opinions and data contained in all publications are solely those of the individual author(s) and contributor(s) and not of MDPI and/or the editor(s). MDPI and/or the editor(s) disclaim responsibility for any injury to people or property resulting from any ideas, methods, instructions or products referred to in the content.